

1 Analysis of daily river flow fluctuations using Empirical  
2 Mode Decomposition and arbitrary order Hilbert  
3 spectral analysis

4 Yongxiang Huang<sup>b,a,\*</sup>, François G. Schmitt<sup>b</sup>, Zhiming. Lu<sup>a</sup>, Yulu Liu<sup>a</sup>

5 <sup>a</sup>*Shanghai Institute of Applied Mathematics and Mechanics, Shanghai University, 200072*  
6 *Shanghai, China*

7 <sup>b</sup>*Université des Sciences et Technologies de Lille - Lille 1, CNRS, Laboratory of*  
8 *Oceanology and Geosciences, UMR 8187 LOG, 62930 Wimereux, France*

---

9 **Abstract**

In this paper we presented the analysis of two long time series of daily river flow data, 32 years recorded in the Seine river (France), and 25 years recorded in the Wimereux river (Wimereux, France). We applied a scale based decomposition method, namely Empirical Mode Decomposition (EMD), on these time series. The data were decomposed into several Intrinsic Mode Functions (IMF). The mean frequency of each IMF mode indicated that the EMD method acts as a filter bank. Furthermore, the cross-correlation between these IMF modes from Seine river and Wimereux river demonstrated correlation among the large scale IMF modes, which indicates that both rivers are likely to be influenced by the same maritime climate event of Northern France. As a confirmation we found that the large scale parts have the same evolution trend. We finally applied arbitrary order Hilbert spectral analysis, a new technique coming from turbulence studies and time series analysis, on the flow discharge of Seine river. This new method provides an amplitude-frequency representation of the original time series, giving a joint

---

\*Corresponding author. Tel.: +33 321 992935; Fax: +33 321 992901.  
*Preprint submitted to Journal of Hydrology, March 26, 2009*  
Email addresses: yongxianghuang@gmail.com (Yongxiang Huang),  
francois.schmitt@univ-lille1.fr (François G. Schmitt), zmlu@shu.edu.cn  
(Zhiming. Lu), ylliu@staff.shu.edu.cn (Yulu Liu)

pdf  $p(\omega, \mathcal{A})$ . When marginal moments of the amplitude are computed, one obtains an intermittency study in the frequency space. Applied to river flow discharge data from the Seine river, this shows the scaling range and characterizes the intermittent fluctuations over the range of scales from 4.5 to 60 days, between synoptic and intraseasonal scales.

10 *Key words:* River flow, Empirical Mode Decomposition, Hilbert Spectral  
11 Analysis, scaling, intermittency

---

## 12 **1. Introduction**

13 A better understanding of river flow fluctuations is of sharp practical  
14 importance, e.g. for ecosystem studies (transport properties), and for flood  
15 understanding and forecasting. River flows fluctuate on many different scales:  
16 at small scales, river turbulence induces stochastic fluctuations and at larger  
17 scales (from days to years) the river flow fluctuations are the result of com-  
18 plex nonlinear interactions between rainfall processes, topography and geog-  
19 raphy (Schumm, 2005). They are also impacted by solar forcing and other  
20 large scale variations of the climate system (Mauas et al., 2008). Daily river  
21 flow time series thus show fluctuations possessing stochastic properties, as  
22 well as deterministic forcing resulting from seasonal or annual meteorological  
23 and climatic cycles.

24 Since Hurst (Hurst, 1951) revealed the long-range dependent property in  
25 river flow, associated to a scaling property, researchers have tried different  
26 methods to characterize the (multi)scaling properties in river flows (Hurst  
27 et al., 1965; Tessier et al., 1996; Pandey et al., 1998; Jánosi and Gallas,  
28 1999; Kantelhardt et al., 2003, 2006; Livina et al., 2003a,b; Koscielny-Bunde

29 et al., 2006; Mauas et al., 2008). Below we quickly review the approaches  
30 undertaken in these studies.

31 Tessier et al. (1996) analyzed the relation between rainfall and river  
32 flow of 30 rivers and basins in France. They used the double trace moment  
33 technique to characterize the multifractal properties. They found that a  
34 scaling break occurs at a scale about 16 days. They argued that the rain  
35 field itself is the source of the river flow, therefore typical scales in the rain  
36 field will also be present in the river flow.

37 Dahlstedt and Jensen (2005) investigated the Danube and the Missis-  
38 sippi river flows and levels by using finite-size-scaling hypothesis (Aji and  
39 Goldenfeld, 2001). They considered the river flow basin size  $L$  from differ-  
40 ent locations. They characterized the multiscaling properties of river flow  
41 and level records by considering the relative and general relative scaling  
42 (or Extended-Self-Similarity and Generalized Extended-Self-Similarity in the  
43 turbulent community). They found that the Fourier spectrum may be dif-  
44 ferent from location to location due to the size effect of the basin area.

45 More recently, several authors applied the so-called detrended fluctua-  
46 tion analysis (DFA) and its multifractal version to describe the scaling and  
47 multiscaling properties of river flows (Kantelhardt et al., 2003; Livina et al.,  
48 2003a,a; Kantelhardt et al., 2006; Koscielny-Bunde et al., 2006; Livina et al.,  
49 2007; Zhang et al., 2008a,b). Livina et al. (2003a,b) argued that the climate  
50 is strongly forced by the periodic variations of the Earth with respect to  
51 the state of the solar system. The seasonal variations in the solar radiation  
52 cause periodic changes in temperature and precipitations, which eventually  
53 lead to a seasonal periodicity of river flows. The Fourier and structure func-

54 tion analyses are impacted by this strong periodicity (Livina et al., 2003a,b;  
55 Kantelhardt et al., 2003; Koscielny-Bunde et al., 2006). According to these  
56 authors, the DFA approach is an efficient method to eliminate the trend  
57 effects.

58 Koscielny-Bunde et al. (2006) found that the Hurst number  $H$  varies from  
59 river to river between  $0.55 \sim 0.95$  in a non-universal manner independent of  
60 the size of the basin. They found that at large time scales,  $F_q(s)$  scales as  
61  $s^{h(q)}$ , and they further proposed a simple function form with two parameters  
62  $a$  and  $b$ ,  $h(q) = 1/q - [\ln a^q + b^q]/[q \ln(2)]$  to describe the scaling exponent  
63  $h(q)$  of all moments (Kantelhardt et al., 2003). Kantelhardt et al. (2006)  
64 also found that the Hurst number  $H$  estimated from 99 precipitation and  
65 42 river runoff records data are not consistent with the hypothesis that the  
66 scaling is universal with an exponent close to 0.75 (Hurst et al., 1965; Peters  
67 et al., 2002).

68 We consider here a method devoted to deal with any nonlinear time series,  
69 which has never been applied to river flow data. In this paper, we apply  
70 the empirical mode decomposition (EMD) and the arbitrary order Hilbert  
71 spectral analysis (HSA) (Huang et al., 2008), which is an extended version  
72 of Hilbert-Huang transform, on river flow discharge fluctuations data. The  
73 arbitrary order HSA is a new methodology, which provides the joint pdf  
74 of the instantaneous frequency  $\omega$  and the amplitude  $\mathcal{A}$ , to characterize the  
75 scale invariant properties directly in amplitude-frequency space (Huang et al.,  
76 2008). We first introduce the EMD and arbitrary order HSA methodology in  
77 section 2. We then present two long records of river flow discharge data from  
78 the Seine river and the Wimereux river in section 3. The analysis results are

79 presented in section 4. Section 5 is a discussion and section 6 summarizes  
80 the main results of this paper.

## 81 **2. Methodology**

### 82 *2.1. Empirical Mode Decomposition*

83 The starting point of the EMD is that most of the signals are multi-  
84 components, which means that there exist different scales simultaneously  
85 (Cohen, 1995; Huang et al., 1998, 1999). The signal can be considered as a  
86 superposition of fast oscillations to slower ones at a very local level (Rilling  
87 et al., 2003; Flandrin and Gonçalvès, 2004). Time series analysis methods  
88 generally consider a characteristic scale explicitly or implicitly. For example,  
89 the Fourier analysis characterizes the scale by the length of one period of  
90 sine (or cosine) wave. Then an integration operator is applied to extract the  
91 components information. Fourier analysis is thus an energy based method:  
92 only when the component contains enough energy, it can be detected by  
93 such method (Huang et al., 1998; Huang, 2005). The characteristic scale for  
94 the present EMD approach is defined as the distance between two successive  
95 maxima (or minima) points. This scale based definition gives the EMD a  
96 very local ability (Huang et al., 1998, 1999). According to the above defi-  
97 nition of a characteristic scale, the so-called Intrinsic Mode Function (IMF)  
98 is then proposed to approximate the mono-component signal, which satis-  
99 fies the following two conditions: (i) the difference between the number of  
100 local extrema and the number of zero-crossings must be zero or one; (ii) the  
101 running mean value of the envelope defined by the local maxima and the  
102 envelope defined by the local minima is zero.

103 The Empirical Mode Decomposition algorithm is proposed to extract the  
104 IMF modes from a given time series (Huang et al., 1998, 1999; Flandrin  
105 et al., 2004). The first step of the EMD algorithm is to identify all the local  
106 maxima (resp. minima) points for a given time series  $x(t)$ . Once all the  
107 local maxima points are identified, the upper envelope  $e_{\max}(t)$  (resp. lower  
108 envelope  $e_{\min}(t)$ ) is constructed by a cubic spline interpolation. The mean  
109 between these two envelopes is defined as  $m_1(t) = (e_{\max}(t) + e_{\min}(t))/2$ . The  
110 first component is estimated by  $h_1(t) = x(t) - m_1(t)$ . Ideally,  $h_1(t)$  should be  
111 an IMF as expected. In reality, however,  $h_1(t)$  may not satisfy the condition  
112 to be an IMF. We take  $h_1(t)$  as a new time series and repeat the shifting  
113 process  $j$  times, until  $h_{1j}(t)$  is an IMF. We thus have the first IMF component  
114  $C_1(t) = h_{1j}(t)$  and the residual  $r_1(t) = x(t) - C_1(t)$  from the data  $x(t)$ .  
115 The shifting procedure is then repeated on residuals until  $r_n(t)$  becomes a  
116 monotonic function or at most has one local extreme point. This means that  
117 no more IMF can be extracted from  $r_n(t)$ . Thus, with this algorithm we  
118 finally have  $n - 1$  IMF modes with one residual  $r_n(t)$ . The original data  $x(t)$   
119 is then rewritten as

$$x(t) = \sum_{i=1}^{n-1} C_i(t) + r_n(t) \quad (1)$$

120 A stopping criterion has to be introduced in the EMD algorithm to stop the  
121 shifting process (Huang et al., 1998, 1999; Rilling et al., 2003; Huang et al.,  
122 2003; Huang, 2005). However, this is beyond our topic here: for more details  
123 about the EMD method, we refer to Huang et al. (1998, 1999); Rilling et al.  
124 (2003); Huang et al. (2003); Flandrin et al. (2004); Flandrin and Gonçalves  
125 (2004); Huang (2005); Rilling and Flandrin (2008).

126 *2.2. Hilbert Spectra Analysis*

127 Having obtained the IMF modes from the EMD algorithm, one can apply  
 128 the associated Hilbert Spectral Analysis (HSA) (Cohen, 1995; Long et al.,  
 129 1995; Huang et al., 1998, 1999) to each IMF component  $C_i$  to extract the  
 130 energy-time-frequency information from the data. The Hilbert transform is  
 131 written as

$$\tilde{C}_i(t) = \frac{1}{\pi} P \int_0^\infty \frac{C_i(t')}{t-t'} dt' \quad (2)$$

132 where  $P$  means the Cauchy principle value (Cohen, 1995; Long et al., 1995).  
 133 From this, we can construct the analytic signal,  $\mathbb{C}_i(t)$ , defined as

$$\mathbb{C}_i(t) = C_i(t) + j\tilde{C}_i(t) = \mathcal{A}_i(t)e^{j\theta_i(t)} \quad (3)$$

134 in which  $\mathcal{A}_i(t) = |\mathbb{C}_i(t)| = [C_i(t)^2 + \tilde{C}_i^2(t)]^{1/2}$  and  $\theta_i(t) = \arctan(\tilde{C}_i(t)/C_i(t)$ .  
 135 Hence the corresponding instantaneous frequency can be defined as

$$\omega_i = \frac{d\theta_i(t)}{dt} \quad (4)$$

136 The original signal is then finally represented as (excluding the residual  $r_n(t)$ )

$$x(t) = \text{RP} \sum_{i=1}^N \mathcal{A}_i(t)e^{j\theta_i(t)} = \text{RP} \sum_{i=1}^N \mathcal{A}_i(t)e^{j \int \omega_i(t) dt} \quad (5)$$

137  
 138 where RP means real part. This approach allows Frequency-Modulation and  
 139 Amplitude-Modulation simultaneously (Huang et al., 1998, 1999). Then the  
 140 Hilbert spectrum  $H(\omega, t) = \mathcal{A}^2(\omega, t)$  is introduced, representing the energy  
 141 in a time frequency space, and we define the Hilbert marginal spectrum as

$$h(\omega) = \int_0^\infty H(\omega, t) dt \quad (6)$$

142 This is similar to the Fourier spectrum, since it corresponds to the energy  
143 associated to the frequency (Huang et al., 1998, 1999).

144 The combination of EMD and HSA is also sometimes called Hilbert-  
145 Huang transform. It provides an alternative powerful tool to analyze non-  
146 stationary and nonlinear time series. The main advantage of EMD over  
147 traditional approaches is its complete self-adaptiveness and its very local  
148 ability both in physical space and frequency space. Therefore it is especially  
149 suitable for nonlinear and nonstationary time series analysis (Huang et al.,  
150 1998, 1999). Since its introduction, this method has attracted a large inter-  
151 est (Huang, 2005). It has been shown to be an efficient method to separate  
152 a signal into a trend and small scale fluctuations on a dyadic bank (Wu  
153 and Huang, 2004; Flandrin et al., 2004; Flandrin and Gonçalves, 2004); it  
154 has also been applied to many fields including physiology (Su et al., 2008),  
155 geophysics (Jánosi and Müller, 2005), climate studies (Solé et al., 2007), me-  
156 chanical engineering (Chen et al., 2004), acoustics (Loutridis, 2005), aquatic  
157 environment (Schmitt et al., 2007, 2008) and turbulence (Huang et al., 2008),  
158 to quote a few.

### 159 *2.3. Arbitrary Order Hilbert Spectral Analysis*

160 HSA represents the energy-time-frequency information  $H(\omega, t)$  at a very  
161 local level. We can then define the joint pdf  $p(\omega, \mathcal{A})$  of the instantaneous  
162 frequency  $\omega$  and the amplitude  $\mathcal{A}$  for all the IMF modes (Long et al., 1995;  
163 Huang et al., 2008). Thus the corresponding Hilbert marginal spectrum is  
164 rewritten as

$$h(\omega) = \int_0^{\infty} p(\omega, \mathcal{A}) \mathcal{A}^2 d\mathcal{A} \quad (7)$$

165 The above equation is no more than the second order statistical moment. In  
 166 a recent paper we have generalized the above definition into arbitrary order  
 167 moment, which is written as (Huang et al., 2008)

$$\mathcal{L}_q(\omega) = \int_0^\infty p(\omega, \mathcal{A}) \mathcal{A}^q d\mathcal{A} \quad (8)$$

168 where  $q \geq 0$ . In case of scale invariance we can write

$$\mathcal{L}_q(\omega) \sim \omega^{-\xi(q)} \quad (9)$$

169 where  $\xi(q)$  is the corresponding scaling exponent. Due to the integration,  
 170  $\xi(q) - 1$  corresponds to  $\zeta(q)$  the scaling exponent of structure functions,  
 171 which is classically written as

$$\langle \Delta x_\tau^q \rangle \sim \tau^{\zeta(q)} \quad (10)$$

172 where  $\Delta x_\tau = |x(t + \tau) - x(t)|$  is the amplitude of the increments at scale  $\tau$ .

173 We provide here some comments on the arbitrary order HSA methodol-  
 174 ogy. If one represents the structure function analysis in Fourier space, one  
 175 may find that it measures the scale invariance by an indirect way, which is  
 176 influenced by the trend or strong large scales. The increment operates the  
 177 data on very local level in the physical domain, but nevertheless, it is still  
 178 a global operator in the frequency domain. On the contrary, the present  
 179 methodology has completely self-adaptiveness and very local ability both in  
 180 the physical and frequency domains (Huang et al., 2008).

### 181 **3. Seine River and Wimereux River**

182 The Seine river is the third largest river in France. Its length is 776 km,  
 183 and its basin is 78650 km<sup>2</sup>. It is economically important for France, with 25%

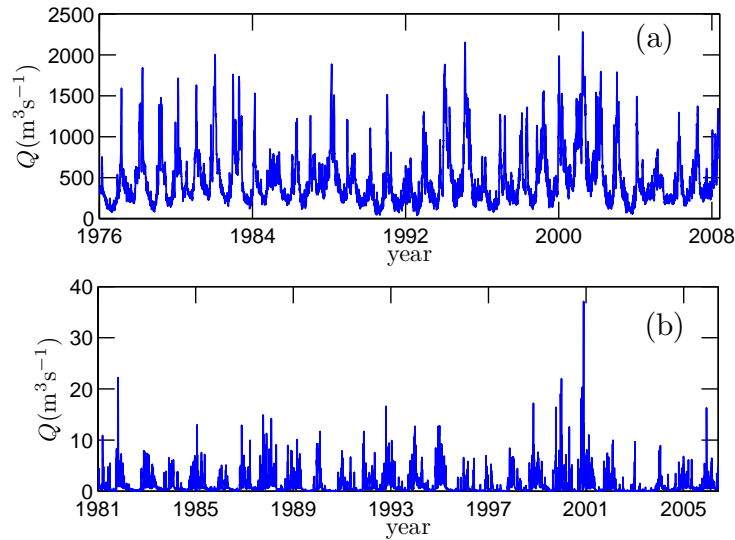


Figure 1: The river flow discharge time series of (a) Seine River, recorded from 1 January 1976 to 28 April 2008, (b) Wimereux river, recorded from 1 January 1981 to 27 May 2006. The data illustrate clear strong annual cycles with huge fluctuations. The total lengths are 11828 and 9278 data points for the Seine river and the Wimereux river, respectively.

184 of its population as well as 40% of its industry and agriculture concentrated  
 185 in and around it (Dauvin, 2007). The flow data is provided by the Service de  
 186 Navigation de la Seine (SNS). This corresponds to daily flow data  $Q$  ( $\text{m}^3\text{s}^{-1}$ ),  
 187 recorded from 1 January 1976 to 28 April 2008. There are 11828 data values,  
 188 with some missing values due to interruptions for maintenance or because of  
 189 the failure of measuring devices. Due to the local ability of HSA approach,  
 190 which is performed through spline interpolation, the missing values in the  
 191 time series do not change the results, since the method can be applied even  
 192 for irregular sampling. The data are shown in Fig. 1 (a), demonstrating  
 193 some large fluctuations at all scales. The mean and standard deviation of  
 194 the discharge are  $488 \text{ m}^3\text{s}^{-1}$  and  $349 \text{ m}^3\text{s}^{-1}$ , respectively. This figure shows a

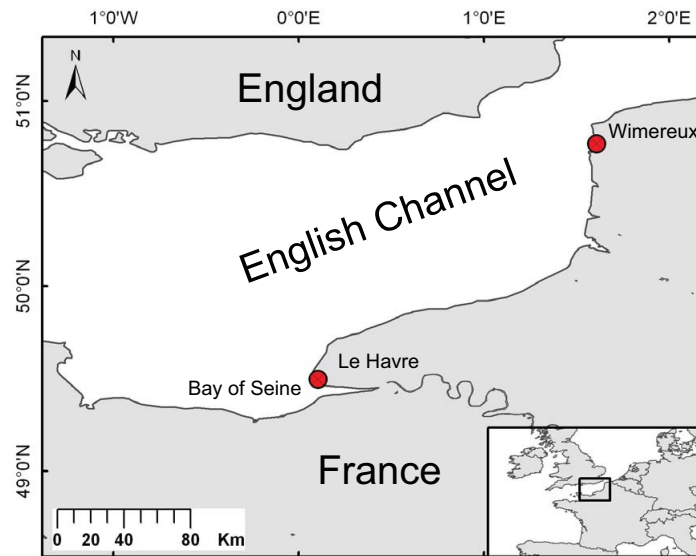


Figure 2: A map showing the location of the Seine river and the Wimereux river, in the eastern English Channel. The distance between them about 300 km.

195 complex and stochastic behavior, with a visible strong annual cycle.

196 The Wimereux river is a small river in the North of France. Its length  
 197 is 22 km, and its basin is 78 km<sup>2</sup>. It can have strong fluctuations due to  
 198 fast increase of the flow in case of heavy rain. The daily flow discharge is  
 199 recorded from 1 January 1981 to 27 May 2006, with a total length of 9278  
 200 points values with some missing, see Fig. 1 (b). The mean and standard  
 201 deviation of the discharge data are 1.02 m<sup>3</sup>s<sup>-1</sup> and 1.73 m<sup>3</sup>s<sup>-1</sup>.

202 Figure 2 shows the location of these two rivers, where the Seine river is  
 203 represented as a solid line. The Wimereux river is too small to be displayed  
 204 in the same figure. The difference between these two rivers is clear: the Seine  
 205 river is a real big one, and the Wimereux river is much smaller and strongly  
 206 influenced by the local rainfall conditions. The distance between them is

207 about 300 km, see Fig. 2. Both of them are affected by the same large scale  
 208 climatic factors and belong to the marine west coast climate of Northern  
 209 France. This climate is found on the west coast of middle latitude regions  
 210 and can be quite humid. Indeed it is subject to western wind bringing impor-  
 211 tant variability intermittent clouds, important precipitation and temperate  
 212 temperatures. The direct estimation of the cross correlation between these  
 213 two recorded data is about 0.256, a value that may be contaminated by the  
 214 small scale uncorrelated fluctuations. We will apply to these two data sets  
 215 by the EMD method in the following section.

## 216 4. Results

### 217 4.1. EMD results

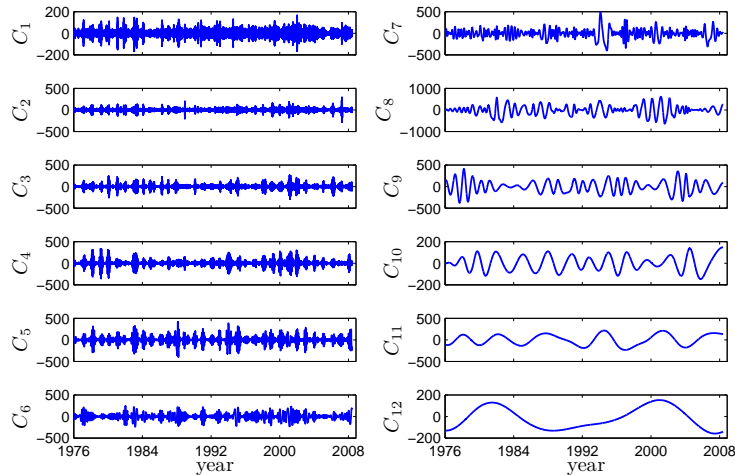


Figure 3: IMF modes (excluding the residual) from EMD for the Seine river. Here the data are taken from 1 January 1976 to 28 April 2008. The characteristic scale is increasing with the mode index number  $n$ .

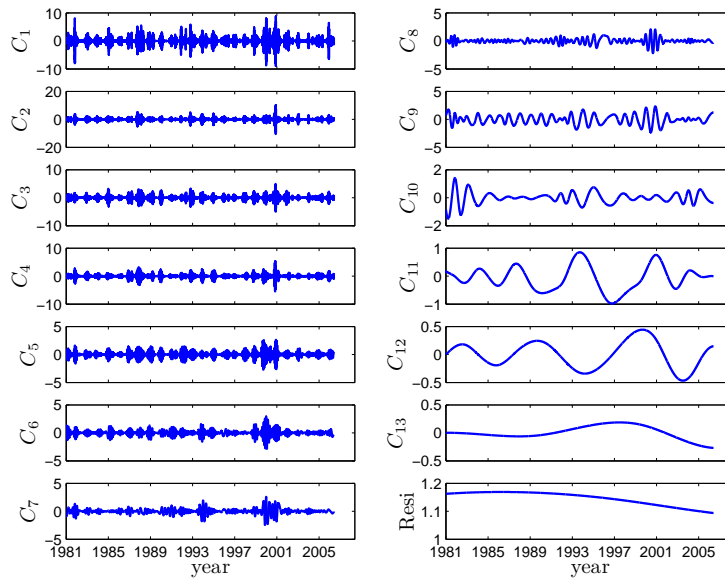


Figure 4: IMF modes from EMD for the Wimereux river. Here the data are taken from 1 January 1981 to 27 May 2006.

218 After the application of the EMD method, the original data is separated  
 219 into several IMF modes. We then represent the IMF modes in Fig. 3 and  
 220 Fig. 4 for the Seine river and the Wimereux river, respectively. For display  
 221 convenience, we exclude the residual for the Seine river. Graphically, one  
 222 can see that the characteristic scale is increasing with the mode index  $n$ .  
 223 Let us note that the number of IMF modes is produced by the algorithm  
 224 and depends on the length and the complexity of the data. In practice,  
 225 based on the dyadic filter bank property of the EMD method, this number  
 226 is usually less than  $\log_2(N)$ , where  $N$  is the length of the data (Flandrin and  
 227 Gonçalves, 2004; Flandrin et al., 2004; Wu and Huang, 2004; Huang et al.,  
 228 2008). First, we estimate the mean frequency  $\bar{\omega}$  of each IMF mode. We use  
 229 the following three definitions of mean frequency  $\bar{\omega}$ . The first one is proposed

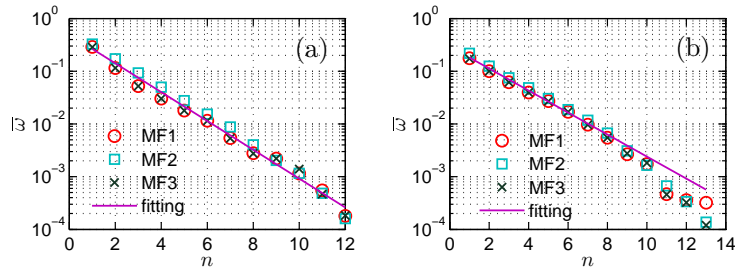


Figure 5: Representation of the mean frequency  $\bar{\omega}$  vs the mode index  $n$  in log-linear view: (a) Seine river, (b) Wimereux river, where the mean frequency  $\bar{\omega}$  are estimated by using Eqs. (11) ( $\circ$ ), (12) ( $\square$ ) and (13) ( $\times$ ), respectively. An exponential law is observed for each representation. The straight line is the least square fit of the data.

Table 1: The mean period (in days) of each IMF mode (excluding the residual) of the Seine river and the Wimereux river, respectively. Here the mean period is estimated as  $\bar{T} = 1/\bar{\omega}$ , where  $\bar{\omega}$  is calculated by Eq. (11). The 8<sup>th</sup> and 9<sup>th</sup> IMF modes of the Seine river and Wimereux river, respectively, are close to the annual cycle.

IMF	1	2	3	4	5	6	7	8	9	10	11	12	13
Seine	3	8	19	33	55	86	185	358	452	869	1823	5551	
Wimereux	5	9	16	25	36	58	103	182	376	574	2149	2785	3125

230 by Huang (Huang et al., 1998), which is written as

$$\bar{\omega}_i = \frac{\int_0^\infty f S_i(f) df}{\int_0^\infty S_i(f) df} \quad (11)$$

231 where  $S_i(f)$  is Fourier spectrum of  $\mathbb{C}_i$ . It is an energy weighted average in  
 232 Fourier space. The second one is given by Flandrin (Flandrin et al., 2004;  
 233 Flandrin and Gonçalves, 2004), which is written as

$$\bar{\omega}_i = \frac{\mathbb{N}^0 - 1}{\mathbb{L}^0} \quad (12)$$

234 where  $\mathbb{N}^0$  is the zero-crossing number, and  $\mathbb{L}^0$  is the distance between the  
 235 first and last zero-crossing. The third one is introduced here for the first

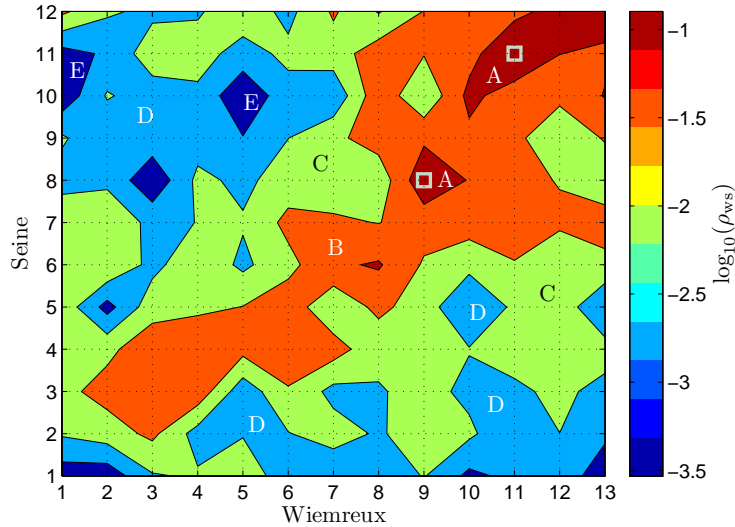


Figure 6: Representation of the cross-correlation  $\rho_{ws}$  between IMF modes from the Seine and Wimereux rivers. The data span is taken from 1 January 1981 to 27 May 2006 for both series. For convenience, we consider the coefficient value  $\log_{10}(\rho_{ws}(i, j))$ . As expected, the annual cycle shows a strong correlation with a coefficient  $\rho_{ws}(9, 8) = 0.426$ . The coefficient of the most correlated modes is  $\rho_{ws}(11, 11) = 0.579$ . These two strong correlations are then marked by  $\square$ .

236 time, and is defined as

$$\bar{\omega}_i = \frac{\int_0^\infty \omega h_i(\omega) d\omega}{\int_0^\infty h_i(\omega) d\omega} \quad (13)$$

237 where  $h_i(\omega)$  is the Hilbert marginal spectrum for the  $i^{\text{th}}$  mode. This definition  
 238 is similar to the first one: it is an energy weighted measurement of the  
 239 mean frequency in Hilbert space. We then represent the mean frequency  $\bar{\omega}$   
 240 estimated by these three definitions (11) ( $\circ$ ), (12) ( $\square$ ) and (13) ( $\times$ ) for  
 241 each mode in Fig. 5 for (a) the Seine river, and (b) the Wimereux river.  
 242 One can see that the two energy weighted estimators give almost the same  
 243 mean frequency. However, they are slightly smaller than the zero-crossing

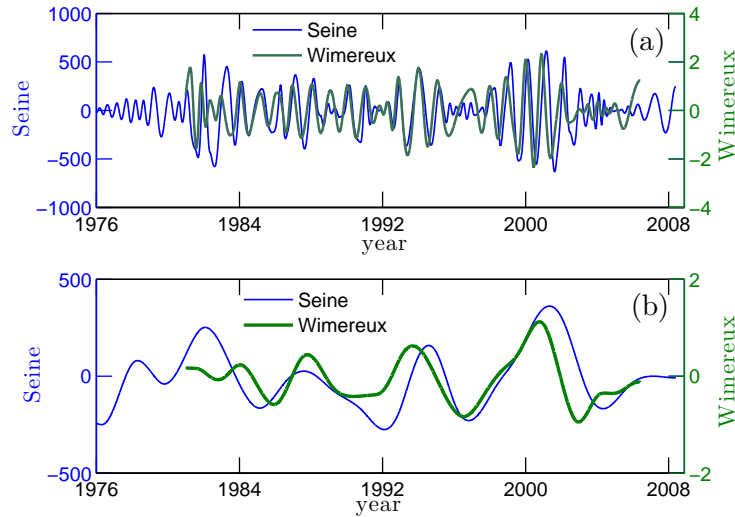


Figure 7: Most correlated IMF modes: (a) the annual cycle mode for the Seine river (thin solid line) and the Wimereux river (thick solid line), (b) the reconstruction of the large scale part for the Seine river (thin solid line) and the Wimereux river (thick solid line). We took the IMF modes 11 ~ 12 from the Seine river and 11 ~ 13 from the Wimereux river, which means periods larger than 3 years, to reconstruct the large scale part. Graphically, they have the same evolution trend on range 1 January 1981 to 28 May 2006.

244 based estimator. Graphically, all these three estimators suggest the following  
 245 exponential law

$$\bar{\omega}(n) \sim \gamma^{-n} \quad (14)$$

246 where  $\gamma_s \simeq 1.88$ ,  $\gamma_w \simeq 1.62$  are estimated by using the least square fitting  
 247 for the Seine river and the Wimereux river, respectively. This result implies  
 248 that the mean frequency of a given mode is  $\gamma$  times larger than the mean  
 249 frequency of next one. We notice that these values are significantly different  
 250 from 2, which would correspond to a dyadic filter bank, which are reported  
 251 for white noise (Wu and Huang, 2004), fractional Gaussian noise (Flandrin  
 252 et al., 2004; Flandrin and Gonçalves, 2004) and turbulence time series (Huang

253 et al., 2008). However, it still indicates that the EMD algorithm acts a filter  
 254 bank here.

255 We list the mean period  $\bar{T}$  (in days) in Table 1, where  $\bar{T} = 1/\bar{\omega}$ . Since  
 256 the three above mentioned mean frequency estimators give almost the same  
 257 value, we thus only present the value estimated by Eq. (11). One can find  
 258 that the EMD approach captures the annual cycle, which is the 8<sup>th</sup> and 9<sup>th</sup>  
 259 mode for the Seine river and Wimereux river, respectively. Both rivers belong  
 260 to the same climate and it is expected that large scale modes are correlated.  
 261 However, the data at daily scale are not (the cross-correlation at this scale  
 262 is 0.256); this is due to the influence of small scales. The cross-correlation  
 263 between two IMF modes is defined as

$$\rho_{ws}(i, j) = \frac{\langle C_{w,i} C_{s,j} \rangle}{\langle C_{w,i}^2 \rangle^{1/2} \langle C_{s,j}^2 \rangle^{1/2}} \quad (15)$$

264 where  $\langle \cdot \rangle$  means ensemble average. The corresponding cross-correlation  $\rho_{ws}(i, j)$   
 265 is then plotted in Fig. 6, where the most correlated modes are marked by  $\square$ .  
 266 The large scale modes are correlated as expected. More precisely, we observe  
 267 a larger cross-correlation between the annual cycle modes,  $\rho_{ws}(9, 8) = 0.426$ ,  
 268 and the most correlation coefficient is  $\rho_{ws}(11, 11) = 0.579$ , with mean pe-  
 269 riods of about 6 and 8 years for the Seine river and the Wimereux river,  
 270 respectively.

271 We then replot the annual cycle for the Seine river (thin solid line) and  
 272 Wimereux river (thick solid line) in Fig. 7 (a). One can find that their shapes  
 273 are almost the same on the range from 1 January 1981 to 28 May 2006. We  
 274 also reconstruct the large scale signal from those modes, with mean period  
 275 larger than 3 years, 11<sup>th</sup> and 12<sup>th</sup> from the Seine river (thin solid line), and  
 276 11<sup>th</sup> to 13<sup>th</sup> from the Wimereux river (thick solid line). The result is shown

277 in Fig. 7 (b). Graphically, they have almost the same shape and evolution  
 278 trend.

279 *4.2. Arbitrary order HSA results*

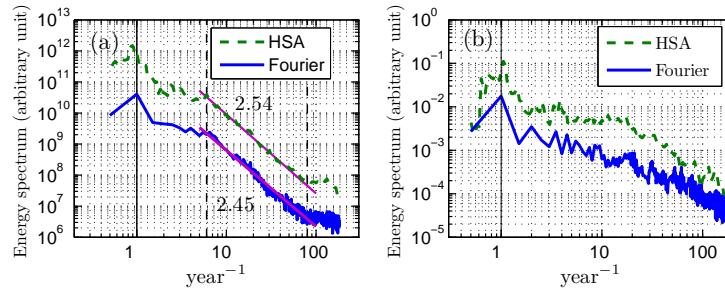


Figure 8: Comparison of the Hilbert marginal spectrum (dashed line) and Fourier spectrum (solid line) for (a) the Seine river, (b) the Wimereux river. For the Seine river, a power law behaviour is observed on the range  $6 < \omega < 80 \text{ year}^{-1}$ , or  $4.5 \sim 60$  days: this range is marked by the vertical dashed lines. The scaling values are 2.54 and 2.45 for Hilbert spectrum and Fourier spectrum, respectively. The vertical solid line indicates the annual cycle.

280 In order to characterize the intermittent properties of river flow fluctu-  
 281 ations, we consider here HSA and arbitrary order HSA analysis. We firstly  
 282 compare the Hilbert marginal spectrum (dashed line) and Fourier spectrum  
 283 (solid line) in Fig. 8 for (a) the Seine river, and (b) the Wimereux river to  
 284 identify the power law range, where the scale invariance holds. For the Seine  
 285 river, both methods capture the annual cycle (vertical solid line) and show  
 286 power law behaviour on the range  $6 < \omega < 80 \text{ year}^{-1}$  or from 4.5 to 60 days,  
 287 with scaling exponent 2.54 and 2.45, respectively. The power law range is  
 288 between synoptic and intraseasonal scales (Zhang, 2005). The latter may be  
 289 linked to the Madden-Julian Oscillation (MJO), since some connection be-

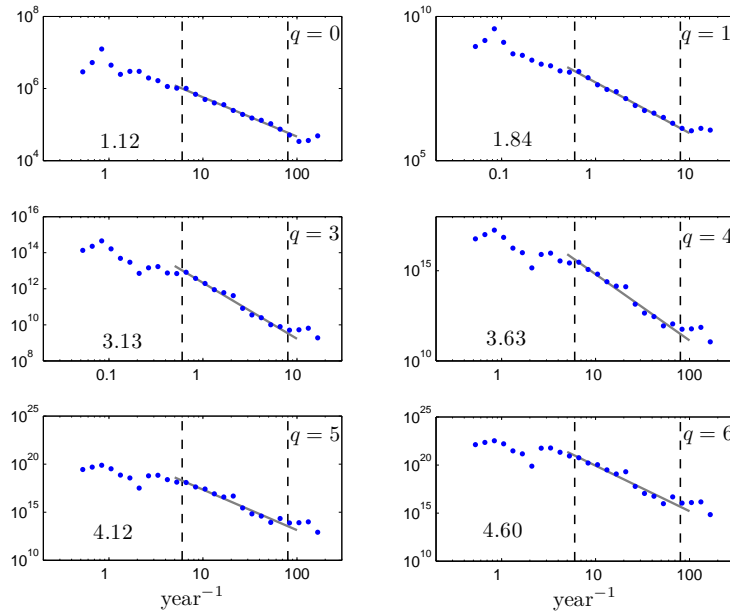


Figure 9: Representation of arbitrary order Hilbert marginal amplitude spectra  $\mathcal{L}_q(\omega)$  for the Seine river, where  $q = 0, 1, 3, 4, 5$  and  $6$ . A power law behaviour is observed in all cases on the range  $6 < \omega < 80 \text{ year}^{-1}$ . The vertical dashed lines indicate the power law range. The corresponding scaling values are shown in each figure.

290 tween and the North Atlantic Oscillation (NAO) and MJO have been found  
 291 (Cassou, 2008). For the Wimereux river, the power law range is less clear.  
 292 We therefore only apply below the arbitrary order HSA analysis on the Seine  
 293 river.

294 Since we are concerned with the scaling property in the above range, we  
 295 thus divide the entire time series into 16 segments, each one has  $2 \times 365$   
 296 points, 2 years each. The arbitrary order Hilbert marginal spectra are shown  
 297 in Fig. 9, where  $q = 0, 1, 3, 4, 5$  and  $6$ . Power law behaviour is then observed  
 298 in all cases on range  $6 < \omega < 80 \text{ year}^{-1}$ , graphically. The corresponding  
 299 scaling exponents  $\xi(q)$  are estimated on this range by using least square

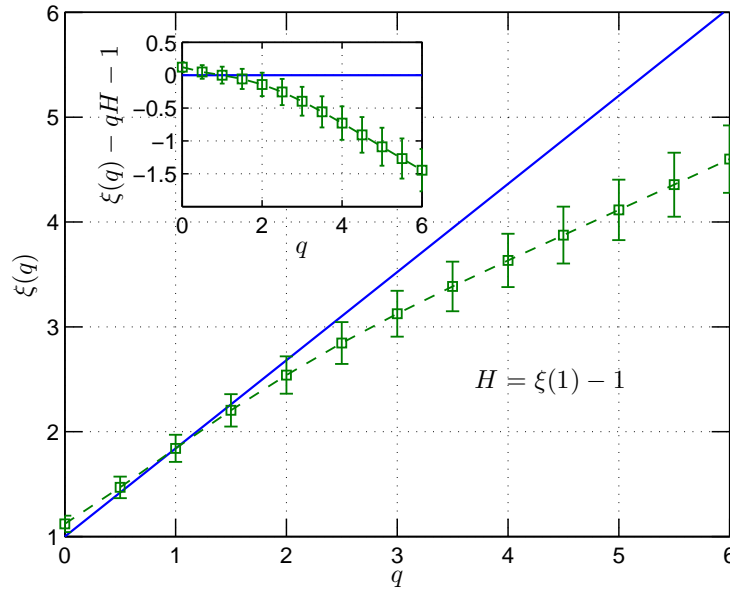


Figure 10: Scaling exponents  $\xi(q)$  ( $\circ$ ) for the Seine river. The inset shows the departure from the reference line  $qH + 1$ , where  $H = \xi(1) - 1$ . The shape of these scaling exponents is concave, which indicates the small scale intermittency nature of river flow.

300 fitting with 95% confidence limit, Fig. 10 shows the scaling exponents  $\xi(q)$   
 301 ( $\circ$ ). Graphically, this curve is concave, which indicates the multifractal  
 302 properties of the river flow discharge (Pandey et al., 1998; Kantelhardt et al.,  
 303 2003, 2006). For comparison, we also show a reference line  $qH + 1$  (solid line),  
 304 where  $H = \xi(1) - 1 = 0.84 \pm 0.08$ , which corresponds to the mono-scaling  
 305 case. The departure from this reference mono-scaling line is then shown in  
 306 inset.

## 307 5. Discussions

308 We compare the above observation with the conventional structure func-  
 309 tion analysis, the traditional way to extract the scaling exponents. We plot

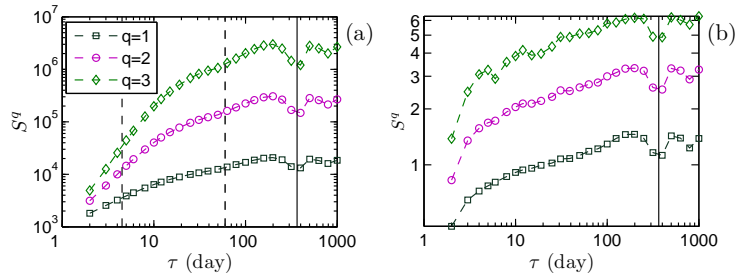


Figure 11: Structure function for (a) the Seine river, and (b) the Wimereux river, where  $q = 1$  ( $\square$ ),  $2$  ( $\circ$ ) and  $3$  ( $\diamond$ ). The vertical dashed lines indicate the range  $4.5 \sim 60$  days. The annual cycle influence is also indicated by the solid line.

310 the result in Fig. 11, where  $q = 1$  ( $\square$ ),  $2$  ( $\circ$ ) and  $3$  ( $\diamond$ ), respectively. Some  
 311 scaling portion are visible on these figures, of a relatively limited amplitude.  
 312 To reveal the scale invariance more clearly, we consider the Extended Self-  
 313 Similarity (ESS) properties, a relative scaling expressed as

$$\langle \Delta x^q \rangle \sim \langle \Delta x \rangle^{\psi(q)} \quad (16)$$

314 where in case of scaling (Eq. 10), we have  $\zeta(q) = H\psi(q)$ . Eq (16) can be  
 315 used to estimate more accurately the exponents  $\psi(q)$ . The ESS is verified  
 316 for the Seine river on range  $2 < \tau < 60$  days, see Fig 12. Figure 13 shows  
 317 the ESS result for the Wimereux river. Graphically, it is scaling and is  
 318 rather scattered. We then show the relative scaling exponents  $\psi(q)$  and the  
 319 normalized scaling exponents  $(\xi(q) - 1)/(\xi(1) - 1)$  in Fig 14. In the mono-  
 320 scaling case and when there is no large scale forcing, they should collapse  
 321 on a solid line  $\psi(q) = q$ . The same approach is applied to the Wimereux  
 322 river. In this case the HSA approach is not displaying any clear scaling  
 323 range. We thus use the ESS approach and compare the resulting curve  
 324  $\psi(q)$  to the one obtained from the Seine river. The Wimereux river scaling

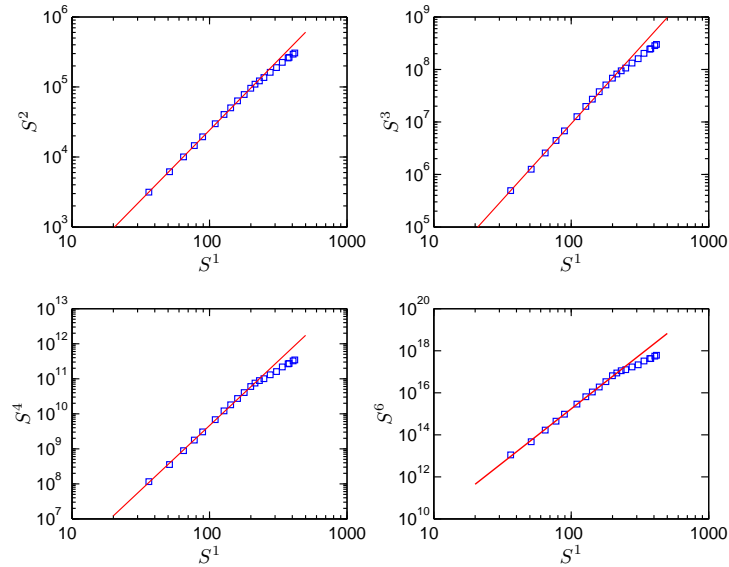


Figure 12: Extended self-similarity test of the Seine river on range  $2 < \tau < 300$  day. The relative scaling is very well captured for all moments.

325 exponents are saturating at  $\psi(q = 1)$ , and the curve is quite different from  
 326 the Seine river. This shows that the Wimereux river is more intermittent  
 327 than the Seine river: which may come from the fact that its catchment basin  
 328 is much smaller, hence its discharge variation can be more rapid. This may  
 329 also be an effect of strong oscillations that reduce the multifractal degree  
 330 (see Telesca et al. (2004b); Bolzan et al. (2009)). It is also interesting to  
 331 see in the same graph the difference between the HSA based exponents and  
 332 structure function's exponents for the Seine river. The discrepancy can be  
 333 interpreted as coming from the influence of the periodic component in the  
 334 time series. Indeed we have shown elsewhere (Huang et al., 2009) that the  
 335 influence of periodic components is stronger on structure function than on  
 336 HSA exponents, which can be linked to the fact that EMD acts a filter

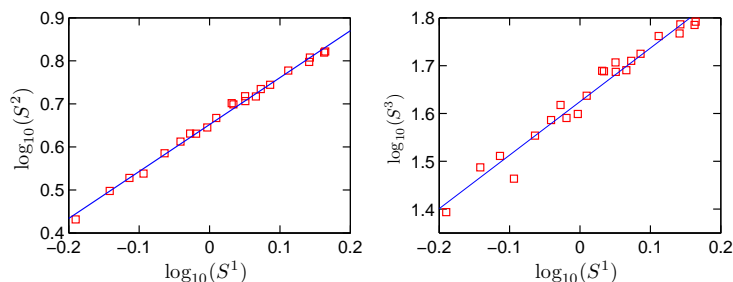


Figure 13: Extended self-similarity test of the Wimereux river on range  $2 < \tau < 300$  day.

337 bank (Flandrin and Gonçalves, 2004; Flandrin et al., 2004; Huang et al.,  
 338 2008; Wu and Huang, 2004). Periodic components tend to increase the value  
 339 of  $\zeta(q)$  relative to the real theoretical curve.

## 340 6. Conclusions

341 In this paper we applied for the first time the EMD methodology to river  
 342 flow time series. Using daily river flow discharge data, 32 years recorded  
 343 in the Seine river (France), and 25 years recorded in the Wimereux river  
 344 (France), we have shown that the time series can be successfully separated  
 345 into several IMF modes. Exponential laws for the mean frequency of each  
 346 mode have been found, with exponents  $\gamma_s = 1.88$  and  $\gamma_w = 1.62$  for the  
 347 Seine river and the Wimereux river, respectively. These values are smaller  
 348 than 2, the value for dyadic filter bank. Even though, it still confirmed that  
 349 the EMD algorithm acts as a filter bank for river flow data. Furthermore,  
 350 strong cross-correlation have been observed between annual cycles and the  
 351 large scale modes having a mean period larger than 3 years. Based on the  
 352 correlation analysis results, we have found that the annual cycle mode and  
 353 the reconstructed large scale part have almost the same evolution trend.

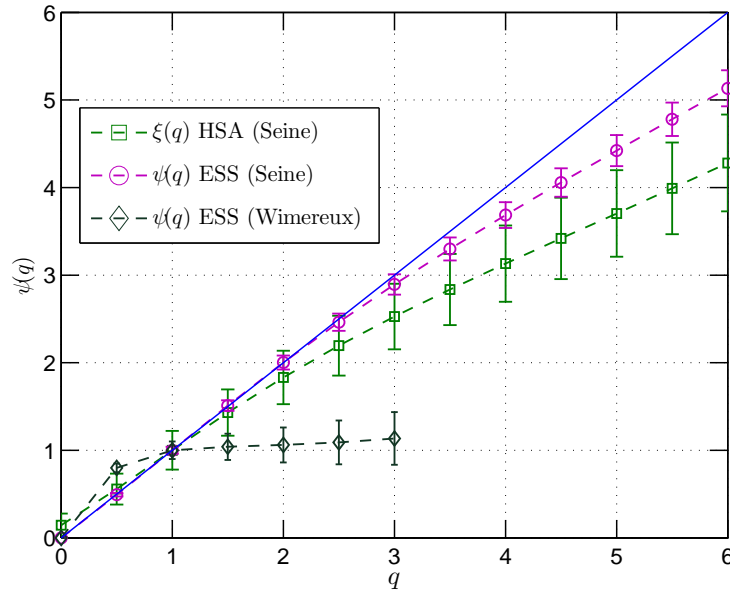


Figure 14: Comparison of the relative scaling exponent  $\psi(q)$  ( $\square$ ) and  $(\xi(q) - 1)/(\xi(1) - 1)$  ( $\circ$ ).

354 We have also characterized the intermittency of the time series over the  
 355 ranges showing scaling properties. For the Seine river, we observed power  
 356 laws for the first six order Hilbert marginal spectra on the range  $6 < \omega <$   
 357  $80 \text{ year}^{-1}$  or  $4.5 \sim 60$  days, between synoptic and intraseasonal scales. The  
 358 corresponding scaling exponents  $\xi(q)$  indicate the small scale multifractal  
 359 nature of the river flow data analyzed here. The differences obtained using  
 360 the structure functions approach and the frequency based HSA approach have  
 361 been emphasized, which is especially clear for large order moments associated  
 362 to the more active fluctuations. We have interpreted this difference as coming  
 363 from the strong annual cycle which has more influence on structure functions  
 364 scaling exponents than on the HSA approach. We have also compared the  
 365 scaling exponents estimated from the ESS method, for the Seine river and

366 Wimereux river; the much smaller exponents obtained for the Wimereux  
367 river express a higher degree of multifractality, which was interpreted as  
368 coming from the inertia associated to the large scale basin for the Seine  
369 river, whereas small rivers such as the Wimereux river may be more sensitive  
370 to local precipitation events.

371 Several previous studies have considered scaling properties of river flows  
372 using other methods such as rescaled range analysis, trace moments, double  
373 trace moments, wavelet analysis, multifractal detrended fluctuation analy-  
374 sis (MFDA). We applied here a new method which gives results similar to  
375 the classical methods (structure functions, wavelet analysis, MFDA) for frac-  
376 tional Brownian motion or pure multifractal processes Huang et al. (2009).  
377 However, we have shown in the same paper that strong deterministic forcing  
378 had important influence on classical methods, whereas the HSA approach  
379 was much more stable and presented less influence Huang et al. (2009). This  
380 method seems hence more appropriate for environmental time series that pos-  
381 sess often strong periodic components superposed to scaling regimes. The  
382 origin of this stability property is the adaptative and local approach which  
383 is at the heart of the HSA method.

384 We have compared here two rivers of very different size and catchment  
385 basin in order to compare their scaling properties. One of the objectives of  
386 scaling analyses of river flow time series is indeed to detect some differences  
387 among rivers, but also to evaluate some universality, i.e. some general simi-  
388 larity in statistical properties. This was done for normalized pdfs Dahlstedt  
389 and Jensen (2005), for river flow volatilities Livina et al. (2003a,b), and for  
390 scaling regimes Tessier et al. (1996) or multifractal parameters Pandey et al.

391 (1998). We hope that the method presented in this paper, which we claim to  
392 be well adapted to environmental time series, will help this quest for universal  
393 properties of river flow scaling statistics.

### 394 **Acknowledgments**

395 This work is supported in part by the National Natural Science Founda-  
396 tion of China (No.10672096 and No.10772110) and the Innovation Founda-  
397 tion of Shanghai University. Y. H. is financed in part by a Ph.D. grant from  
398 the French Ministry of Foreign Affairs and by part from university of Lille  
399 1. Financial support was provided by the program Seine Aval: this work  
400 is a contribution to ZOOSEINE project funded by Seine-Aval IV program.  
401 The EMD Matlab codes used in this paper are written by P. Flandrin from  
402 laboratoire de Physique, CNRS & ENS Lyon (France): [http://perso.ens-](http://perso.ens-lyon.fr/patrick.flandrin/emd.html)  
403 [lyon.fr/patrick.flandrin/emd.html](http://perso.ens-lyon.fr/patrick.flandrin/emd.html).

### 404 **References**

- 405 Aji, V., Goldenfeld, N., 2001. Fluctuations in Finite Critical and Turbulent  
406 Systems. *Phys. Rev. Lett.* 86 (6), 1007–1010.
- 407 Bolzan, M., Rosa, R., Sahai, Y., 2009. Multifractal analysis of low-latitude  
408 geomagnetic fluctuations. *Ann. Geophys* 27, 569–576.
- 409 Cassou, C., 2008. Intraseasonal interaction between the Madden–Julian Os-  
410 cillation and the North Atlantic Oscillation. *Nature* 455 (7212), 523–527.
- 411 Chen, J., Xu, Y. L., Zhang, R. C., 2004. Modal parameter identification of

- 412 Tsing Ma suspension bridge under Typhoon Victor: EMD-HT method. J.  
413 Wind Eng. Ind. Aerodyn. 92 (10), 805–827.
- 414 Cohen, L., 1995. Time-frequency analysis. Prentice Hall PTR Englewood  
415 Cliffs, NJ.
- 416 Dahlstedt, K., Jensen, H., 2005. Fluctuation spectrum and size scaling of  
417 river flow and level. Physica A 348, 596–610.
- 418 Dauvin, J. C., 2007. Paradox of estuarine quality: Benthic indicators and  
419 indices, consensus or debate for the future. Mar. Pollut. Bull. 55 (1-6),  
420 271–281.
- 421 Flandrin, P., Gonçalves, P., 2004. Empirical Mode Decompositions as Data-  
422 Driven Wavelet-Like Expansions. Int. J. Wavelets, Multires. Info. Proc.  
423 2 (4), 477–496.
- 424 Flandrin, P., Rilling, G., Gonçalves, P., 2004. Empirical mode decomposition  
425 as a filter bank. IEEE Sig. Proc. Lett. 11 (2), 112–114.
- 426 Huang, N. E., 2005. Hilbert-Huang Transform and Its Applications. World  
427 Scientific, Ch. 1. Introduction to the hilbert huang transform and its re-  
428 lated mathematical problems, pp. 1–26.
- 429 Huang, N. E., Shen, Z., Long, S. R., Wu, M. C., Shih, H. H., Zheng, Q., Yen,  
430 N., Tung, C. C., Liu, H. H., 1998. The empirical mode decomposition and  
431 the Hilbert spectrum for nonlinear and non-stationary time series analysis.  
432 Proc. R. Soc. London 454 (1971), 903–995.

- 433 Huang, N. E., Shen, Z., Long, S. R., et al., 1999. A new view of nonlinear  
434 water waves: The Hilbert Spectrum . *Annu. Rev. Fluid Mech.* 31 (1),  
435 417–457.
- 436 Huang, N. E., Wu, M. L., Long, S. R., Shen, S. S. P., Qu, W., Gloersen, P.,  
437 Fan, K. L., 2003. A confidence limit for the empirical mode decomposition  
438 and Hilbert spectral analysis. *Proc. R. Soc. London* 459 (2037), 2317–2345.
- 439 Huang, Y., Schmitt, F. G., Lu, Z., Liu, Y., 2008. An amplitude-frequency  
440 study of turbulent scaling intermittency using hilbert spectral analysis.  
441 *Europhys. Lett.* 84, 40010.
- 442 Huang, Y., Schmitt, F. G., Lu, Z., Liu, Y., 2009. Analyse de l’invariance  
443 d’échelle de séries temporelles par la décomposition modale empirique et  
444 l’analyse spectrale de hilbert. *Traitement du Signal* (in press).
- 445 Hurst, H., Black, R., Simaika, Y., 1965. Long-term storage: an experimental  
446 study.
- 447 Hurst, H. E., 1951. Long-term Storage Capacity of Reservoirs. *Trans. Am.*  
448 *Soc. Civ. Eng.* 116, 770–808.
- 449 János, I., Gallas, J., 1999. Growth of companies and waterlevel fluctuations  
450 of the river Danube. *Physica A* 271 (3), 448–457.
- 451 János, I., Müller, R., 2005. Empirical mode decomposition and correlation  
452 properties of long daily ozone records. *Phys. Rev. E* 71 (5), 56126.
- 453 Kantelhardt, J., Rybski, D., Zschiegner, S., Braun, P., Koscielny-Bunde, E.,  
454 Livina, V., Havlin, S., Bunde, A., 2003. Multifractality of river runoff and

- 455 precipitation: comparison of fluctuation analysis and wavelet methods.  
456 *Physica A* 330 (1-2), 240–245.
- 457 Kantelhardt, J., Koscielny-Bunde, E., Rybski, D., Braun, P., Bunde, A.,  
458 Havlin, S., 2006. Long-term persistence and multifractality of precipitation  
459 and river runoff records. *J. Geophys. Res.* 111.
- 460 Koscielny-Bunde, E., Kantelhardt, J., Braun, P., Bunde, A., Havlin, S.,  
461 2006. Long-term persistence and multifractality of river runoff records:  
462 Detrended fluctuation studies. *J. Hydrol.* 322 (1-4), 120–137.
- 463 Livina, V., Ashkenazy, Y., Braun, P., Monetti, R., Bunde, A., Havlin, S.,  
464 2003a. Nonlinear volatility of river flux fluctuations. *Phys. Rev. E* 67 (4),  
465 42101.
- 466 Livina, V., Ashkenazy, Y., Kizner, Z., Strygin, V., Bunde, A., Havlin, S.,  
467 2003b. A stochastic model of river discharge fluctuations. *Physica A* 330 (1-  
468 2), 283–290.
- 469 Livina, V., Kizner, Z., Braun, P., Molnar, T., Bunde, A., Havlin, S., 2007.  
470 Temporal scaling comparison of real hydrological data and model runoff  
471 records. *J. Hydrol.* 336 (1-2), 186–198.
- 472 Long, S. R., Huang, N. E., Tung, C. C., Wu, M. L., Lin, R. Q., Mollo-  
473 Christensen, E., Yuan, Y., 1995. The Hilbert techniques: an alternate  
474 approach for non-steady time series analysis. *IEEE Geoscience and Remote  
475 Sensing Soc. Lett.* 3, 6–11.
- 476 Loutridis, S. J., 2005. Resonance identification in loudspeaker driver units:  
477 A comparison of techniques. *Appl. Acoust.* 66 (12), 1399–1426.

- 478 Mauas, P. J. D., Flamenco, E., Buccino, A. P., 2008. solar forcing of the  
479 stream flow of a continental scale south american river. *Phys. Rev. Lett.*  
480 101, 168501.
- 481 Pandey, G., Lovejoy, S., Schertzer, D., 1998. Multifractal analysis of daily  
482 river flows including extremes for basins of five to two million square kilo-  
483 metres, one day to 75 years. *J. Hydrol.* 208 (1-2), 62–81.
- 484 Peters, O., Hertlein, C., Christensen, K., 2002. A complexity view of rainfall.  
485 *Phys. Rev. Lett.* 88 (1), 018701.
- 486 Rilling, G., Flandrin, P., Gonçalvès, P., 2003. On empirical mode decompo-  
487 sition and its algorithms. *IEEE-EURASIP Workshop on Nonlinear Signal*  
488 *and Image Processing.*
- 489 Rilling, G., Flandrin, P., 2008. One or two frequencies? The empirical mode  
490 decomposition answers. *IEEE Trans. Signal Process.*
- 491 Schmitt, F. G., Huang, Y. X., Lu, Z. M., Zongo, S. B., Molinero, J. C.,  
492 Liu, Y. L., 2007. Analysis of nonlinear biophysical time series in aquatic  
493 environments: scaling properties and empirical mode decomposition. In:  
494 *Nonlinear Dynamics in Geosciences.* edited by A. Tsonis and J. Elsner.  
495 Springer, pp. 261–280.
- 496 Schmitt, F. G., Huang, Y. X., Lu, Z. M., Liu, Y. L., Fernandez, N.,  
497 2008. Analysis of velocity fluctuations and their intermittency proper-  
498 ties in the surf zone using empirical mode decomposition. *J. Marine Syst.*  
499 DOI:10.1016/j.jmarsys.2008.11.012.

- 500 Schumm, S., 2005. *River Variability and Complexity*. Cambridge University  
501 Press.
- 502 Solé, J., Turiel, A., Llebot, J., 2007. Using empirical mode decomposition to  
503 correlate paleoclimatic time-series. *Nat. Hazard Earth Sys. Sci.* 7, 299–307.
- 504 Su, Z.-Y., Wang, C.-C., Wu, T., Wang, Y.-T., Feng-Cheng, T., 2008. Instan-  
505 taneous frequency-time analysis of physiology signals: the application of  
506 pregnant women’s radial artery pulse signals. *Physica A* 387, 485–494.
- 507 Telesca, L., Lapenna, V., Macchiato, M., 2004b. Mono-and multi-fractal in-  
508 vestigation of scaling properties in temporal patterns of seismic sequences.  
509 *Chaos, Solitons and Fractals* 19 (1), 1–15.
- 510 Tessier, Y., Lovejoy, S., Hubert, P., Schertzer, D., Pecknold, S., 1996. Multi-  
511 fractal analysis and modeling of rainfall and river flows and scaling, causal  
512 transfer functions. *J. Geophys. Res.* 101, 26427–26440.
- 513 Wu, Z., Huang, N. E., 2004. A study of the characteristics of white noise  
514 using the empirical mode decomposition method. *Proc. R. Soc. London*  
515 460, 1597–1611.
- 516 Zhang, C., 2005. Madden-Julian Oscillation. *Rev. Geophys.* 43, 36.
- 517 Zhang, Q., Xu, C., Chen, Y., Yu, Z., 2008a. Multifractal detrended fluc-  
518 tuation analysis of streamflow series of the Yangtze River basin, China.  
519 *Hydrol. Process.*, DOI: 10.1002/hyp.7119.
- 520 Zhang, Q., Xu, C. Y., Liu, C. L., Chen, Y. D., 2008b. Multifractal analysis

521 of streamflow records of the east river basin (pearl river), china. Physica  
522 A, DOI: 10.1016/j.physa.2008.11.025.